Developmental Cell
Article

A Direct Role for FMRP in Activity-Dependent Dendritic mRNA Transport Links Filopodial-Spine Morphogenesis to Fragile X Syndrome

Jason B. Dictenberg,[1,2,3,*] Sharon A. Swanger,[4] Laura N. Antar,[1] Robert H. Singer,[1,2,5] and Gary J. Bassell[4,5,*]
[1]Department of Neuroscience
[2]Department of Anatomy and Structural Biology
Albert Einstein College of Medicine, Bronx, NY 10461, USA
[3]Department of Biological Sciences, Hunter College, City University of New York, 695 Park Avenue, New York, NY 10065, USA
[4]Departments of Cell Biology and Neurology, Emory University, Atlanta, GA 30322, USA
[5]These authors contributed equally to this work
*Correspondence: Dictenberg@genectr.hunter.cuny.edu (J.B.D.), gbassel@emory.edu (G.J.B.)
DOI 10.1016/j.devcel.2008.04.003

SUMMARY

The function of local protein synthesis in synaptic plasticity and its dysregulation in fragile X syndrome (FXS) is well studied, however the contribution of regulated mRNA transport to this function remains unclear. We report a function for the fragile X mental retardation protein (FMRP) in the rapid, activity-regulated transport of mRNAs important for synaptogenesis and plasticity. mRNAs were deficient in glutamatergic signaling-induced dendritic localization in neurons from *Fmr1* KO mice, and single mRNA particle dynamics in live neurons revealed diminished kinesis. Motor-dependent translocation of FMRP and cognate mRNAs involved the C terminus of FMRP and kinesin light chain, and KO brain showed reduced kinesin-associated mRNAs. Acute suppression of FMRP and target mRNA transport in WT neurons resulted in altered filopodia-spine morphology that mimicked the FXS phenotype. These findings highlight a mechanism for stimulus-induced dendritic mRNA transport and link its impairment in a mouse model of FXS to altered developmental morphologic plasticity.

INTRODUCTION

An emerging theme in the study of molecular mechanisms of learning and memory suggests an important function for the spatio-temporal control of gene expression at the synapse. Interestingly, altered expression of a single mRNA-binding protein (mRBP), FMRP, results in fragile X syndrome (FXS), a highly prevalent form of inherited mental retardation, and contributes significantly to autism spectrum disorders (Penagarikano et al., 2007). FMRP demonstrates selective affinity for mRNA, including its own transcript and other targets important for neuronal development and plasticity (Penagarikano et al., 2007), and is transported in a stimulus-induced manner within dendrites and at spine synapses (Antar et al., 2004) where it is associated with polyribosomes and represses translation (Penagarikano et al., 2007). FMRP is also itself translated within isolated synaptic fractions (Weiler et al., 1997) and in turn, affects translation of mRNA targets, suggesting potential for fine-tuning of local translational control at synapses. In a mouse model of FXS, *Fmr1* knockout (KO) neurons display excess basal translation, yet lack of stimulus-induced translation (Lu et al., 2004; Muddashetty et al., 2007; Zalfa et al., 2003). KO mice exhibit excessive immature dendritic spines, altered learning and behavior, and increased group I metabotropic glutamate receptor (mGluR)-dependent LTD, a form of plasticity that requires protein synthesis (Bagni and Greenough, 2005). Since altered translation of mRNAs has not been observed in situ, our knowledge of how FMRP affects translation in neurons remains limited to biochemically heterogeneous synapse fractions. One mechanism by which FMRP could affect translation is through selective delivery of mRNAs to dendritic translation sites in response to synaptic activity, however the contribution of mRBPs to localization remains poorly understood.

Diverse neuronal signaling pathways can induce the localization of mRNAs (Bramham and Wells, 2007; Dictenberg and Singer, 2008), and mRBPs may serve to link subcellular trafficking of mRNA targets to local translation sites (Kiebler and Bassell, 2006). While details of FMRP function in translational regulation are known (Vanderklish and Edelman, 2005), a potential role for FMRP in mRNA localization has not been directly addressed. Previous low resolution, nonquantitative in situ histological methods failed to detect gross changes in mRNA localization to dendrites in neurons lacking FMRP (Steward et al., 1998). However a more sensitive FISH approach revealed alterations in the steady-state abundance of two FMRP target mRNAs in the molecular layer of hippocampus derived from KO brain, suggesting a role for FMRP in either mRNA transport or stability (Miyashiro et al., 2003; Zalfa et al., 2007).

To explore a role for FMRP in dendritic mRNA localization we quantitatively examined several FMRP target mRNAs in dendrites of hippocampal neurons in response to neuronal activity. We report a deficiency in mGluR-induced mRNA localization in neurons derived from KO mice, and show that the motility of select FMRP target mRNAs important for synapse function is altered. This was measured directly using both fixed cells and

living neurons by visualizing GFP-labeled mRNAs. We describe a molecular mechanism whereby FMRP acts as an adaptor for kinesin light chain to promote stimulus-induced mRNA transport, and observe a widespread uncoupling of FMRP target mRNAs from kinesin in KO brains. Acute suppression of FMRP transport in wild type (WT) neurons resulted in both diminished mRNA transport and a significant increase in the length and number of dendritic filopodia-spine protrusions that is similar to the phenotype observed in the mouse model and in humans with FXS. We propose that an alteration in stimulus-induced synaptic localization and transport kinetics of FMRP target mRNAs involved in synaptogenesis and plasticity may contribute to translational and synaptic defects observed in FXS.

RESULTS

FMRP Functions in Stimulus-Induced Dendritic mRNA Localization

We previously observed increased dendritic transport of FMRP and associated mRNAs (referred to as messenger-ribonucleoprotein particles or mRNPs) upon stimulation of mGluR with DHPG (Antar et al., 2004, 2005). Since FMRP colocalized with known target mRNAs, we have investigated its role in mRNA transport. Here, the localization of several mRNA targets of FMRP, as well as nontargets, were compared in both WT and KO hippocampal cultures.

In response to mGluR stimulation, total polyadenylated (polyA) mRNA was increased in dendrites by ~1.5 to 2-fold in both WT and KO cultures, indicating no gross defects in mRNA transport in KO neurons (Figure S1A, see the Supplemental Data available with this article online; $p < 0.01$, $n = 12$). This was in contrast to the localization of *MAP1b* and *CaMKIIα* mRNAs, which are both translationally regulated by FMRP and encode proteins critical for neurite outgrowth and synapse function (Lu et al., 2004; Muddashetty et al., 2007). *MAP1b* mRNA (Figure 1A) was increased ~4-fold ($p < 0.001$, $n = 16$) in response to DHPG in WT, while *CaMKIIα* mRNA (Figure 1B) increased ~2-fold ($p < 0.01$, $n = 15$). However, in KO neurons the mRNAs did not increase above unstimulated levels (*MAP1b*, $p > 0.25$, $n = 15$; *CaMKIIα*, $p > 0.25$, $n = 17$). We did not observe significantly decreased dendritic levels of *CaMKIIα* or *MAP1b* mRNAs in unstimulated KO neurons compared to WT. However, in KO neurons the signal appeared more diffuse compared to granules observed in WT (Figures 1A and 1B), suggesting altered mRNP structure in the absence of FMRP (Aschrafi et al., 2005). The specificity of the localization response to mGluR was underscored by a lack of differences observed in dendritic *β-actin* mRNA abundance using this paradigm (Figure 1C, $p > 0.15$, $n = 11$-13), both in WT and KO cells, as *β-actin* mRNA localization was previously shown to respond to neurotrophin (Zhang et al., 2001) and NMDA (Tiruchinapalli et al., 2003) receptor stimulation, and does not associate with FMRP (Muddashetty et al., 2007).

Further inspection of mRNA targets of FMRP showed an interesting panel of mRNA localization defects similar to that observed for *MAP1b* and *CaMKIIα*. The mRNAs for *RGS5* and *SAPAP4*, both implicated in the regulation of postsynaptic receptor signaling (Gold et al., 1997; Takeuchi et al., 1997) and whose mRNAs associate with FMRP (Brown et al., 2001; Miyashiro et al., 2003), were also significantly increased (~2-fold; *RGS5*, $p < 0.05$, $n = 15$; *SAPAP4*, $p < 0.01$, $n = 16$) by mGluR activation in WT but not KO neurons (Figure S1B, Figure 1D; *RGS5*, $p > 0.20$, $n = 15$; *SAPAP4*, $p > 0.25$, $n = 17$). The mRNA target of FMRP, *GABA-A-receptor δ* subunit (*GABAR-δ*) (Miyashiro et al., 2003) was significantly increased by ~2-fold in WT dendrites in response to DHPG ($p < 0.01$, $n = 13$), but not in KO (Figure 1E; $p < 0.05$, $n = 15$). Although we also observed an increase in *GABAR-δ* mRNA in KO upon DHPG, the magnitude was small (26% increase) compared to the WT response (81% increase, $p < 0.01$, $n = 13$–15). However, another proposed target of FMRP, *Arc* mRNA, was not significantly increased in either WT or KO neurons under these conditions (Figure S1C, $p > 0.20$, $n = 14$-15). To further ensure that the mRNA signals were not due to individual cell-to-cell variation or culture conditions, we normalized the *SAPAP4* mRNA in situ signals to both dendritic MAP2 fluorescence and synapsin puncta number, which similarly showed significant increases in mRNA levels after stimulation in WT but not KO neurons (Figures S1D and S1E; $n = 16$–17, $p < 0.05$ for *SAPAP4*/MAP2, $p < 0.0001$ for *SAPAP4*/synapsin).

The in situ results suggested that either mRNA targets of FMRP were diminished in dendritic transport or the stability of mRNAs was decreased upon DHPG stimulation. To directly test the loss of FMRP on mRNA transport kinetics, we used the MS2-GFP system to visualize movements of a reporter for the *CaMKIIα* mRNA in live neurons cultured from both WT and KO brain. This reporter construct contains the whole 3′UTR, which is necessary for dendritic localization of *CaMKIIα* mRNA in vivo (Miller et al., 2002) and sufficient for localization in cultured neurons (Rook et al., 2000). Neurons were transfected with *CaMKIIα*-MS2-GFP and imaged in the presence of DHPG. mRNA-GFP particles were tracked over two-minute intervals and the mean square displacement (MSD), a measure of the average distance of travel, of each particle along with the percent motile particles was calculated. Strikingly, there was a significant difference in the kinetics of mRNA movements between the two genotypes (Figure 2A; $p < 0.02$, $n = 307$ particles; Movies S1 and S2). On average 23% of *CaMKIIα* mRNA particles were motile in WT neurons, while only 5% of mRNA particles in KO neurons exhibited vectorial trajectories (Figure 2B). Consistent with a known biochemical interaction of *CaMKIIα* mRNA and FMRP, we observed *CaMKIIα*-MS2-GFP mRNA particles colocalized with endogenous FMRP in WT neurons using FISH to the MS2 mRNA sequence (Figure 2C; Figure S1F).

mGluR Activates Dendritic FMRP Transport through Kinesin Light Chain

To better understand the mechanism of FMRP-mediated mRNA transport in neurons, we analyzed motor interactions. Classic pelleting experiments revealed a nucleotide-dependent association of FMRP with taxol-stabilized microtubules (Figure S2A). Rapid imaging of living neurons expressing FMRP-GFP revealed bidirectional transport of granules at rates up to 1.8 μm/s in dendrites, suggesting involvement of both kinesin and dynein-based movements (Figure 3A; Movie S3). This was consistent with coprecipitation data showing an association of FMRP with these motors (Figure S2B) and specifically KLC (see below), which is a major cargo-binding subunit of the KIF5 holoenzyme (KHC and KLC). However another form of kinesin, KIF3 was not

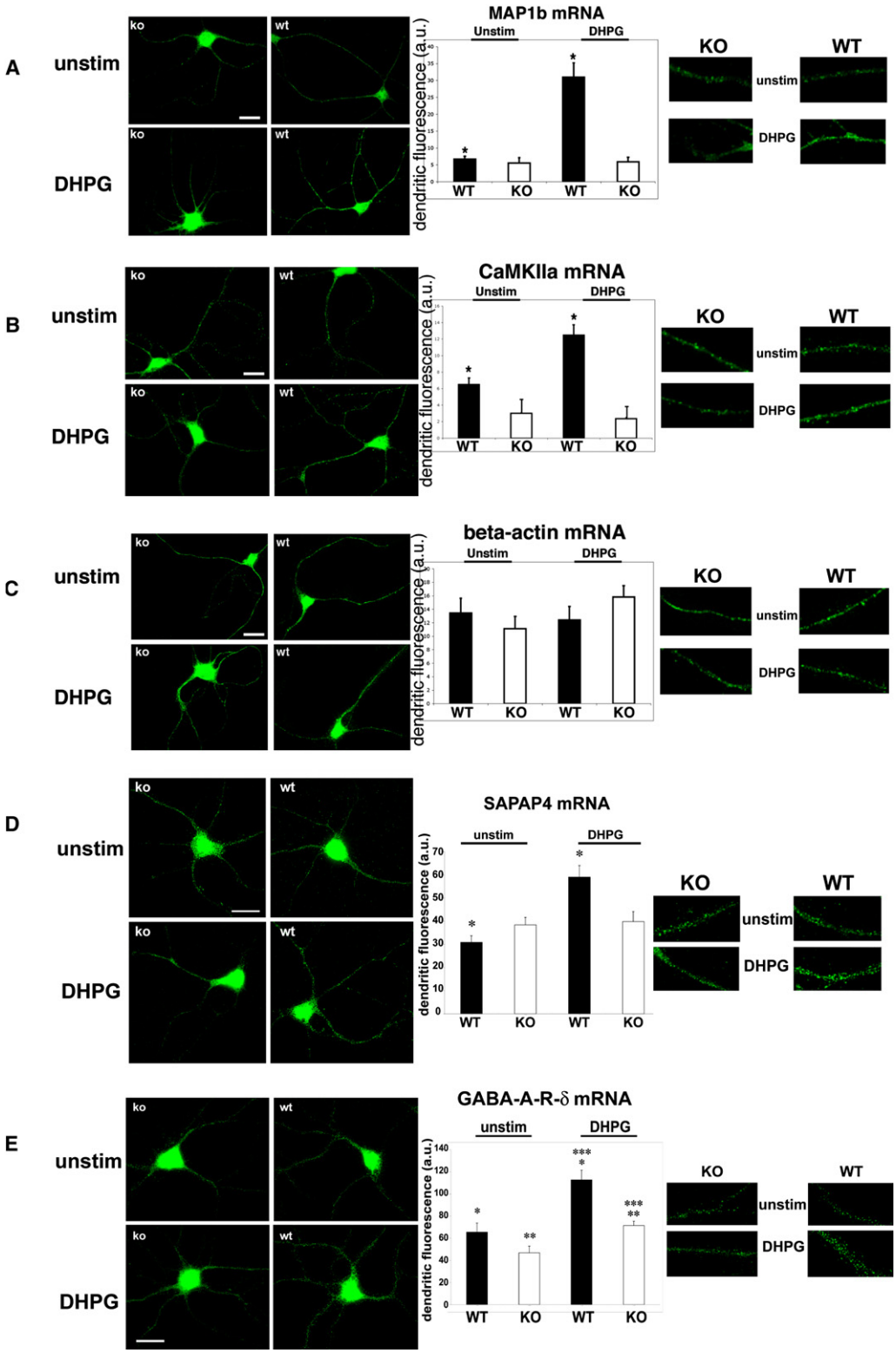

Figure 1. Fluorescence In Situ Hybridization, FISH, of Hippocampal Neurons

(A–D) Neurons from wild type (WT, right panels) or *Fmr1* knockout (KO, left panels) were cultured for 10 days and either not stimulated ("unstim", upper panels) or stimulated with 50 μM DHPG for 15 min ("DHPG", lower panels). Corresponding histograms showing dendritic quantification of FISH experiments are shown to the right. Results for WT (black bars) and KO (white bars) are labeled on the x axis. Close-up images of dendritic signals are shown to the right (in same order). (A) MAP1b mRNA (n = 15–16; *p < 0.001 for unstimulated versus DHPG in WT, p > 0.25 for KO).

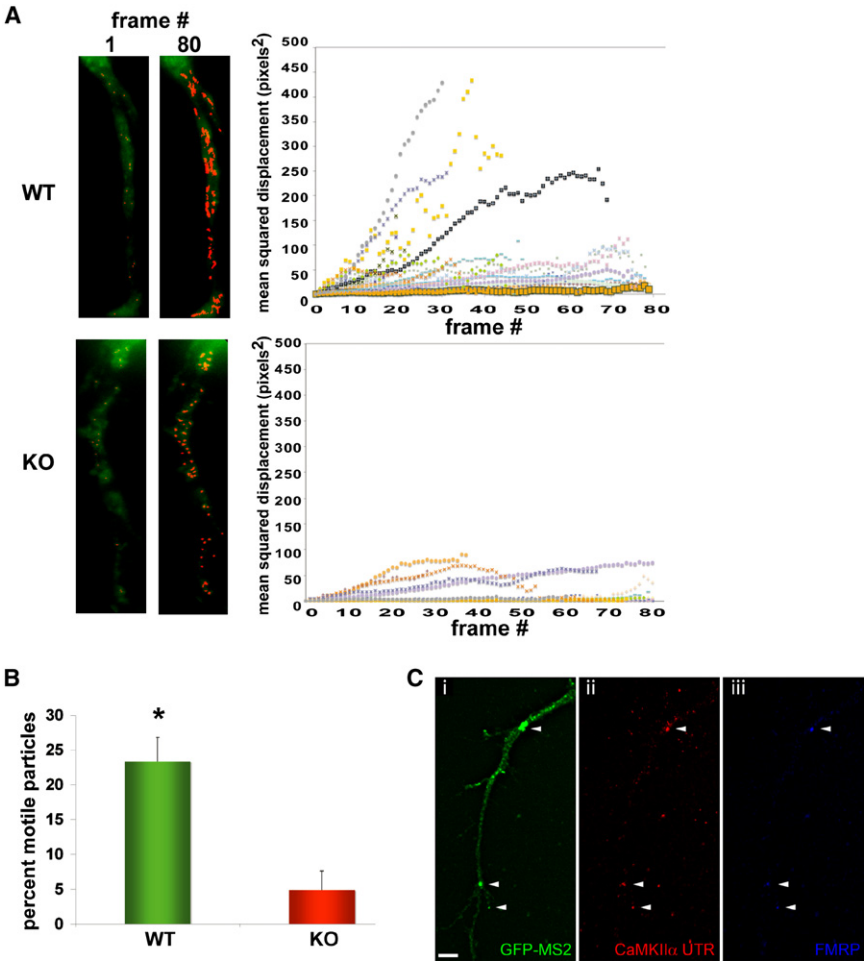

Figure 2. Time-Lapse Analysis of CaMKIIα Reporter mRNA Transport in Live Neurons from *WT* or *Fmr1-KO*

Neurons (10DIV) were transfected with a GFP-MS2-CaMKIIα mRNA reporter, and exposed to DHPG (50 μM, 15 min). mRNA movements were imaged over a two-minute interval, with each frame captured every 1.5 s.

(A) Images (left panels) show the first frame (1) and last frame (80) of the time-lapse series of GFP-MS2-CaMKIIα (green) and highlight the tracked mRNA particles (red). The mean-squared displacement (MSD) of individual particle trajectories were analyzed (graph, right) in WT (upper panels) and KO (lower panels) neurons, and an example of the MSD analysis graphs showing 24 particle trajectories for each genotype are shown at right (24 trajectories on graph; many are overlapping at bottom of graph and obscured by icons). The slope of the individual trajectories approximates the particle velocity, and the MSD measures the trajectory length over time.

(B) Histogram showing the percent of mRNA particles among several movies (n = 6 neurons, 307 particles total, *p < 0.02, mean ± SEM) from both *WT* and *KO* neurons that were motile.

(C) Colocalization of CaMKIIα 3′UTR-MS2-GFP with endogenous FMRP. Fluorescence images of a hippocampal dendrite showing MS2-GFP (i, green), CaMKIIα-MS2 reporter mRNA (ii, red), and FMRP (iii, blue). Arrowheads show three granules in dendrites of this representative neuron triple-labeled where all colocalize, which was determined using 3D deconvolution and image reconstruction (Figure S1F). Scale bar = 5 μm.

significantly associated with FMRP in brain. As a direct test for the role of kinesin in FMRP association with the cytoskeleton in situ, we utilized a highly specific small molecule inhibitor of kinesin (adociasulfate, AS-2), which binds to the motor domain and releases it from microtubules (Sakowicz et al., 1998). Neurons exposed to AS-2 for 15 s showed a significant loss of FMRP in dendrites (Figure S2C; extract with AS-2) compared with either mock extracted (extract only; †$p < 0.01$, $n = 15$) or unextracted (no extract; *$p < 0.005$, $n = 15$) neurons. This same treatment caused specific removal of KIF5 ($p < 0.01$, $n = 8$) with no significant effect on cytoplasmic dynein (Figure S2D, $p > 0.3$, $n = 7$) or on overall MT organization (not shown).

An activity-induced increase in dendritic FMRP localization (Antar et al., 2004) suggested two potential mechanisms involving kinesin: one being an increase in the processivity of kinesin associated with FMRP; an alternative being an increase in the fraction of FMRP associated with kinesin. To test the latter possibility, the fraction of FMRP mRNP granules associated with KIF5 was measured. Cortical neurons cultured from WT mice were extracted either in basal states or after 15 min of mGluR activation, and then probed for FMRP association with KIF5 by immunoprecipitation (IP). Activation of mGluR caused a noticeable increase in the amount of FMRP associated with KIF5 (Figure 3B, western blot). Cultured neurons were also stimulated with DHPG and processed for super-resolution microscopy using image deconvolution (Carrington et al., 1995), and the reconstructed images were used to compare the degree of overlap within the same volume pixels for two distinct isoforms of kinesin. The KIF5 signal correlated significantly with FMRP in dendritic shafts in comparison to KIF3, which did not show a robust correlation

(B) CaMKIIα mRNA (n = 15–17; *$p < 0.01$ for WT, $p > 0.2$ for KO). There was no significant difference in CaMKIIα abundance of unstimulated neurons between WT and KO ($n = 15$, $p > 0.1$).

(C) β-actin mRNA (n = 11–13; $p > 0.2$). Scale bars = 12 μm.

(D–E) FISH for other mRNA targets of FMRP in both WT (right image panels) and KO (left image panels). Representative images shown for unstimulated (upper panels; "unstim") and stimulated (lower panels; DHPG, 50 μM), and close-up images of dendrites are displayed to the right of the histograms (in same order). Histograms (right) showing dendritic fluorescence quantification are shown for WT and KO using probes to (D) SAPAP4 (n = 16–17; $p < 0.01$ for WT, $p > 25$ for KO) and (E) GABA-A receptor δ (n = 13–15; *, ***$p < 0.01$ for unstimulated versus DHPG in WT and for DHPG in WT and KO, **$p < 0.05$ for unstimulated versus DHPG in KO). Scale bars = 12 μm. Values are mean ± SEM.

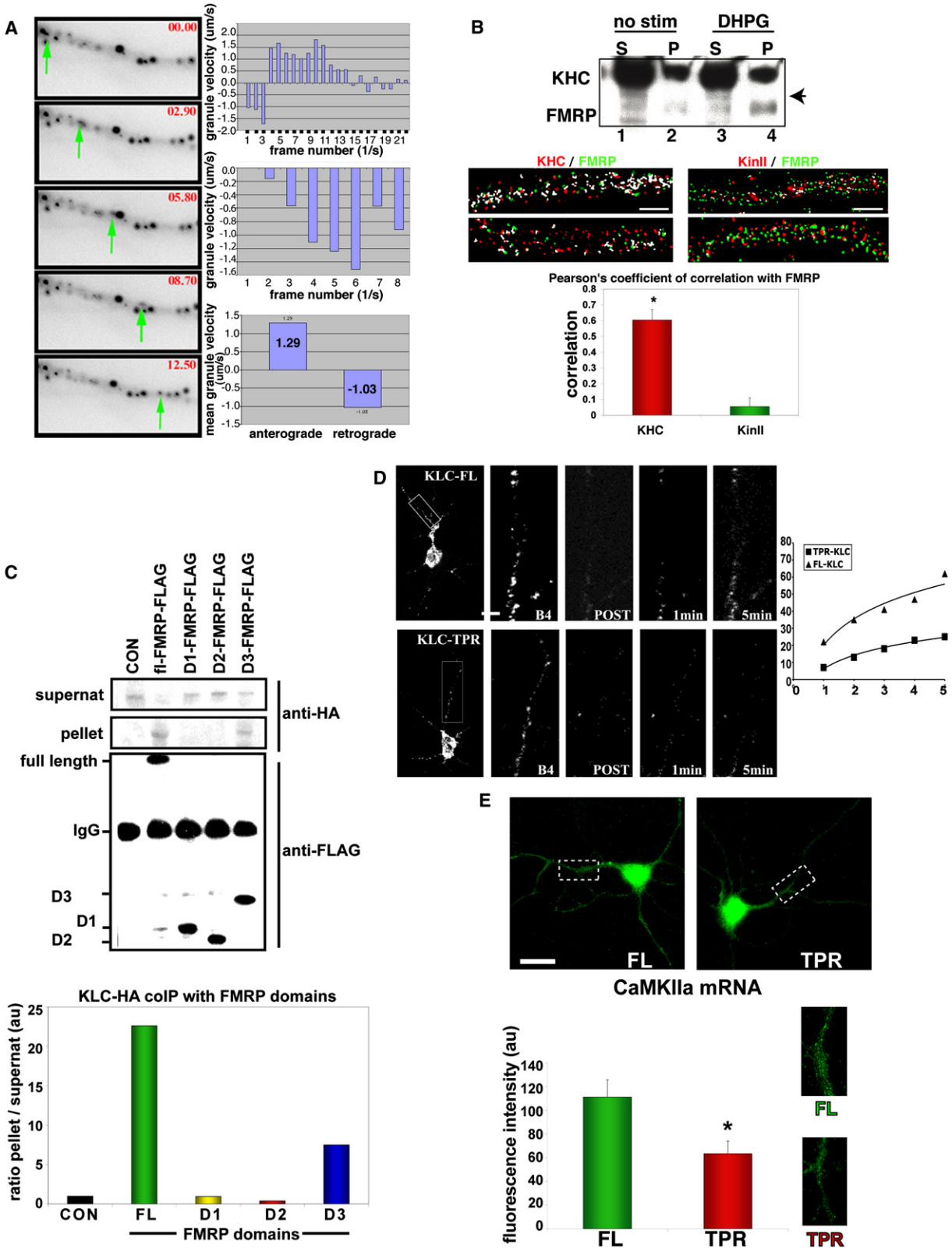

Figure 3. The C Terminus of FMRP Is Involved in Kinesin-Dependent Stimulus-Induced Transport

(A) Rapid FMRP-GFP movements in live hippocampal neurons (10DIV). (Images) Five consecutive image panels (top to bottom, left side) show time points (seconds, red) indicated in the upper-right corner and a green arrow tracing the granule movement. (Histograms) Individual particle velocities (top 2 histograms)

(Figure 3B, image panels and histogram). This was not due to changes in total FMRP levels in response to DHPG (Antar et al., 2004). The stimulus-induced increase in KIF5 association was also observed for a homolog of FMRP, FXR1p, which is known to interact biochemically with the FMRP mRNP (Bagni and Greenough, 2005; Figure S3).

The molecular mechanism of motor attachment to RNA-binding proteins and specifically FMRP remains unknown. Therefore several domains of FMRP were tested for KLC binding in neuronal cell lines (Figure 3C) since we have observed this interaction in brain (Figure S2B). Importantly these cells express type I mGluR and were stimulated with DHPG for 15 min, which increases FMRP association with KLC. Quantitation showed that only the C-terminal domain of FMRP (D3), but not the N-terminal or central domain, could significantly interact with KLC (Figure 3C, histogram). To test the role of KIF5 in FMRP transport in neurons, we used a dominant negative strategy (Verhey et al., 2001). We quantified FMRP-GFP transport rates in neurons cotransfected with either full-length (FL) KLC (control) or the TPR domain, which is able to bind to cargo but lacks the KHC-binding domain. Fluorescence recovery after photobleaching (FRAP) analysis (Figure 3D, image panels) showed that the TPR domain significantly reduced transport kinetics by ~5-fold, with an average time constant (50% recovery) of 1165 s, compared with the control time constant of 237 s (Figure 3D, graph, $n = 6$, $p < 0.005$ at 300 s time point). TPR-KLC had no significant effect on another proposed KIF5 dendritic cargo, the glutamate-receptor interacting protein (GRIP1), which has been shown to interact with KHC (data not shown). We confirmed that transfection of dominant negative KLC-TPR into neurons resulted in a ~4–6-fold increase in cargo-binding domain in both the cell body ($n = 15$, $p < 0.0001$) and in dendrites ($n = 15$, $p < 0.005$) compared with endogenous KLC in untransfected controls (Figure S4A).

To investigate the role of KIF5 in dendritic transport of FMRP mRNA targets, TPR-KLC transfected neurons were stimulated and processed for FISH. Neurons transfected with KLC-TPR showed significantly diminished *CaMKIIα* mRNA localization compared to controls (Figure 3E, 44% lower in TPR-KLC [n] = 22) versus FL-KLC [n = 17], $p < 0.02$). We found a similar effect on the *Fmr1* mRNA itself, which is a known target of FMRP (Ceman et al., 1999; Figure S4B, $p < 0.005$, n = 13–15 cells per treatment). This is in contrast to *MAP2* mRNA, which was not altered by TPR-KLC ($n = 12$) overexpression compared to controls ($n = 14$, FL-KLC) (Figure S4C, $p > 0.22$). Transfection of neurons with KLC constructs was confirmed for all cells and quantification showed that expression levels were similar (Figures S4D and S4E).

FMRP Mediates Association of Target mRNAs with Kinesin

The loss of stimulus-induced mRNA localization in KO neurons suggested that FMRP might play a structural role between mRNAs and molecular motors. One prediction from this model is that loss of FMRP could result in altered target mRNA coupling to kinesin. To test this, WT and KO brains were used to isolate KIF5 and analyze target mRNAs that co-purified (Figure 4). IP of KHC with semiquantitative PCR showed that *SAPAP4* mRNA was significantly reduced in KO brains compared to WT (Figure 4A, WT versus KO lane for KHC-IP), in the range of 50%–70% (Figure S5A). Real-time Q-PCR was performed on a large panel of target mRNAs that revealed different levels (~20%–50%) to which mRNAs were reduced in association with KIF5 in KO brains (Figure 4B, $^*p < 0.05$, $^{**}p < 0.01$, $^{***}p < 0.005$, $^{****}p < 0.0001$, all $n = 8$). The mRNA targets reduced in KIF5 association included genes involved in actin remodeling at synapses (*cofilin phosphatase (PP2Ac); p116-RIP*), synapse-associated signaling (*CaMKIIα*; *DAG1*; *RGS5*) and synapse structure (*SAPAP4; MAP1b*). Not all mRNAs were significantly reduced in KIF5 IPs, as *OCRL1* mRNA was similar in KO brain ($p > 0.05$, $n = 8$). In addition two negative control mRNAs known not to associate with FMRP, *MAP2* and *β-actin* mRNA, were not altered in their association with KIF5 ($p > 0.4$, $n = 8$). A positive control for the assay was *Fmr1* mRNA itself, which showed

were traced on a frame-per-frame basis (granule velocities, μm/sec, + is anterograde, − is retrograde). Average velocities (bottom histogram) were measured for multiple granules (lower graph, right; n = 8, mean values shown).

(B) (Upper panel) Western blot showing KHC and FMRP coIP from cortical cultures. Either nothing (no stim) or DHPG was added to cultures for 15 min and then KHC IP performed. Supts (S) and pellets (P) were analyzed by SDS-PAGE. Arrowhead denotes FMRP band only seen in IP of KHC (other bands in SUPT are likely crossreacting fragile X related proteins or posttranslationally modified FMRP). (Lower Panel) Superresolution 3-D colocalization analysis of kinesin heavy chain and FMRP in dendrites. Hippocampal neurons were cultured (12DIV), fixed, and stained for FMRP (green) and either KIF5 (KHC, left two panels, red) or KIF3 (right two panels, red), and IF images were captured and processed for deconvolution. Images are maximum projections of 3D stacks, and white pixels represent overlap of the two signals. The histogram shows the average Pearson's coefficient of correlation for each antigen pair as calculated (green bar is for KHC/FMRP and red bar is for KIF3/FMRP; $n = 14$, $p < 0.0005$, mean ± SEM). Scale bar = 2 μm.

(C) Domain analysis of FMRP for kinesin interaction. (Top [first] panel: supernat) Quantitative western blot of KLC (anti-HA) shows the supts after the immunoprecipitation (IP) of FMRP domains, with both full-length (FL)-FMRP and C-terminal domain of FMRP (D3, aa 386–585) able to significantly deplete the supt compared to the control (CON, no FMRP protein), N-terminal domain (D1, aa 1–208), or the central domain (D2, aa 290–387) of FMRP. (Second panel: pellet) Western blot against HA shows pellets contain KLC-HA that associate with FMRP by coIP. (Third panel: FMRP pellets) Western blot against FLAG shows the control (CON, no FMRP protein expressed) or IP FL-, D1-, D2-, or D3-FMRP proteins that were used to pull down KLC-HA. (Histogram) HA-KLC bands pulled down for each pellet and the corresponding supt were digitally quantified using the LiCOR quantitative blot system and expressed as a ratio of pellet to supt for each FMRP domain.

(D) Hippocampal neurons (7DIV) showing FRAP of FMRP-GFP in response to DHPG. (Left panel) Images of dendrites subjected to FRAP: Upper series show a low magnification image of a control cell (cotransfected KLC-FL) and the dendritic area bleached (inset box), a higher magnification image of the subregion just before bleach (B4, second panel) and after (third panel), 1 min (fourth panel), and 5 min later (fifth panel). Lower series show the same sequence for KLC-TPR cotransfected with FMRP-GFP. Scale bar = 15 μm. (Right panel) Graph showing the percent recovery (y axis) measured over 300 s (x axis) is shown. Squares represent the KLC-TPR transfected cells while the triangles represent FL-KLC ($n = 6$; $p < 0.005$ at 300 s time point). Calculated time constants of recovery (τ, 50%) are shown on the graph.

(E) (Upper panels) Representative images showing CaMKIIα mRNA FISH for neurons transfected with either FL-KLC (left) or TPR-KLC (right) constructs and stimulated with DHPG for 15 min. Scale bar = 15 μm. (Lower panel) Histogram of CaMKIIα mRNA dendritic abundance in KLC transfected neurons (n = 17–22; $^*p < 0.02$; mean ± SEM). Images to right show close-ups of dendrites from upper-panel images.

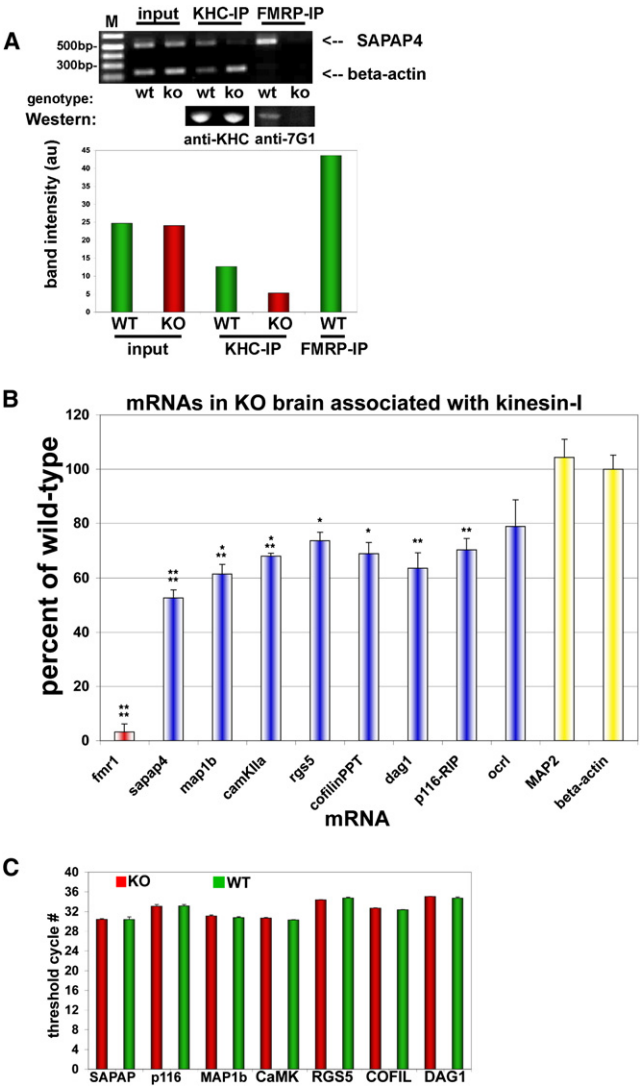

Figure 4. FMRP Target mRNAs Associated with Kinesin

Immunoprecipitation (IP) of KHC was used to analyze associated mRNAs by PCR and determine differences between WT and *Fmr1* KO brain.

(A) (Upper panel) Ethidium gel for semiquantitative RT-PCR products from KHC and FMRP IP pellets using primers for β-actin mRNA (lower bands) and SAPAP4 mRNA (upper bands). "Input" is the input lysate showing starting material for both WT and KO brain. IPs of both kinesin heavy chain (KHC) and FMRP are indicated above the gel, and genotype is indicated below. FMRP IP in KO brain was used to subtract background from other bands, and was ~4% of WT IP. (Middle panel) Western blot of protein pellets showing that the KHC IPs are identical from WT and KO brain. FMRP antibodies (anti-7G1) also reveal that FMRP is able to precipitate in WT but not KO brain (Lower panel: histogram) Quantification of mRNA bands from PCR (upper panel) by digital fluorescence analysis.

(B) Real-time Q-PCR of indicated mRNAs associated with KHC by IP, expressed as a percent of mRNA isolated from KHC in KO compared to WT brain ($n = 8$; $^{*}p < 0.05$; $^{**}p < 0.01$; $^{***}p < 0.005$; $^{****}p < 0.0001$; mean ± SEM).

(C) Real-time Q-PCR analysis of mRNA abundance. Histogram showing that several mRNA targets of FMRP were analyzed for total mRNA levels in both WT (green bars) and KO (red bars) brain derived from P7 mice ($n = 8$, $p \geq 0.4$ [minimum]; values shown are mean ± SEM).

almost zero abundance in KO brain using this method (the first few exons [1–5] of *Fmr1* are still expressed at the 5′ end of the gene in the *KO* where the PCR primers are located). Other controls consisted of an mRNA restricted to the soma, SM51, and GAPDH which were both not different in KIF5 IPs from KO compared to WT (Figure S5B), and were detected at low levels in association with KIF5. Quantification of input mRNA (as well as supernatants after IP, data not shown) by Q-PCR demonstrated that the KIF5-associated mRNAs represented only a fraction of the total mRNA, which was not significantly altered in KO brain for any of the targets examined (Figure 4C).

Transport of FMRP and Target mRNAs Affects the Length and Number of Dendritic Protrusions

Since the loss of FMRP caused pronounced defects in the association of KIF5 with mRNAs important for synapse function and their localization to dendrites, we investigated whether the dendritic protrusion phenotype of FXS was directly affected by target mRNA transport. To test the physiological effect of acute loss of FMRP transport on dendritic morphology in situ, we established a dominant negative approach by overexpression of the KLC-binding C-terminal domain of FMRP (D3) (see Figure 3C), which can compete with endogenous FMRP for KLC binding. Neurons were transfected with either the full-length (FL) FMRP (control) or the D3 construct, together with trace amounts of FL-FMRP-GFP driven by the endogenous promoter as a marker for dendritic transport. Since FL-FMRP can compete with FMRP-GFP for binding to kinesin, we determined a ratio of construct stoichiometry that demonstrated significant FMRP-GFP dendritic localization (it is also likely that multimerization of FMRP diminishes this potentially competitive effect). Compared to the FL protein, overexpression of D3 caused a significant reduction (~7-fold) of FMRP-GFP transport into dendrites (Figure 5A, $p < 0.002$, $n = 23$), while controls (FL-FMRP; $n = 23$) or overexpression of the N-terminal (aa 1–208) or central domain (aa 209–386) of FMRP (see Figure 3C) caused no significant differences (Figure S6A, $p > 0.2$, $n = 15$–19). Under these conditions we have verified that the expression of both constructs were not significantly different (Figure S6B). To analyze endogenous FMRP similarly, we utilized a monoclonal antibody that recognizes a region outside of the C terminus (D3-FMRP). Immunofluorescence staining of D3-FMRP neurons (with CFP as marker) showed diminished dendritic FMRP staining compared to control neurons (CFP only) (Figure 5B, $p < 0.001$, $n = 15$–22). We believe that blocking FMRP transport did not significantly affect other mRNA binding proteins since the overall staining pattern for RNA was not grossly altered (Figure 5B). An antibody to the C terminus of FMRP showed that transfection of D3-FMRP constructs resulted in a ~5-fold increase in expression levels in both the cell body ($n = 9$, $p < 0.001$) and dendrites ($n = 18$, $p < 0.0005$) compared with endogenous FMRP in untransfected neurons (Figure S6C), confirming its ability to act in a dominant manner.

Having established a dominant negative transport assay, we used this approach to assess the effect on dendritic mRNA localization and in turn, spine morphology. The abundance of FMRP target mRNAs was assessed by FISH after activation of mGluR. Examination of transfected neurons showed that *CaMKIIα* mRNA was reduced in D3-FMRP dendrites by approximately half compared to controls (FL-FMRP) after only 36 hr

posttransfection (Figure 5C, $p < 0.01$, $n = 13$). This pattern was similar for another FMRP target mRNA that was reduced almost 3-fold in DHPG-stimulated localization in KO neurons, *SAPAP4* (Figure 5D, $p < 0.001$, $n = 14–15$). However neither *MAP2* (not an FMRP mRNA target), nor *Arc* (not a well-established mRNA target) were significantly affected by overexpression of D3-FMRP (Figure S6D). In all cases we verified the transfection of FL- and D3-FMRP and determined that expression levels were not significantly different between treatments on average (Figures S6E and S6F).

To examine the effect of decreased target mRNA transport on dendritic spine-like protrusion morphology, D3-FMRP was transfected into WT neurons for 36 hr and stimulated with DHPG. Morphology was monitored by cotransfection of trace amounts of CFP-β-actin, and neurons were processed for IF staining of MAP2 (data not shown) to unequivocally identify filopodia and spine protrusions. The morphological similarity between filopodia and spines at this stage made it difficult to distinguish the two simply based on morphology. Therefore protrusions having a long and thin morphology were designated as filopodia-spines as has been described previously (Prange and Murphy, 2001), and represent the major protrusion type during this developmental stage of cultured neurons (Bonhoeffer and Yuste, 2002). Surprisingly, D3 overexpression caused a significant increase in both the length ($p < 0.0001$, $n = 749–852$) and number ($p < 0.005$) of filopodia-spine protrusions compared to control (FL-FMRP) transfected neurons (Figures 5E and 5F). The average number of protrusions increased from 3.0 to 4.8/10 μm dendrite length in D3-FMRP neurons (60%, left side of histogram in Figure 5F), while their average length increased from 2.5 μm in controls to 3.2 μm (28%, right side of histogram). Under these conditions there was no significant alteration in the total number of synapses in either group as assessed by synapsin-positive dendritic puncta (Figure S6G, $p > 0.35$, $n = 12–14$). The effect of reduced FMRP transport on filopodia-spine morphology in WT neurons was strikingly similar to that observed in neurons lacking FMRP, and suggest a mechanistic link between decreases in dendritic target mRNAs important for synaptic function and the dynamics of dendritic protrusions.

DISCUSSION

We have uncovered an aspect of mRNA trafficking into dendrites upon mGluR stimulation that is deficient in neurons lacking FMRP. The mechanism by which this occurs indicates that the C-terminal domain of FMRP can associate with KLC in a dynamic fashion regulated by mGluR activation. These data support a model by which FMRP acts as a molecular adaptor to bind mRNA targets and suppress their translation during kinesin-mediated transport to synaptic sites. In support of this model, a number of mRNA targets are diminished in their association with KIF5 isolated from KO brains. Further work is needed to determine whether FMRP or its partners directly bind KLC and whether these interactions are regulated by kinase/phosphatase signaling pathways downstream of mGluR activation. The stimulus-induced delivery of FMRP mRNPs may play a critical role in regulated protein synthesis-dependent mGluR-mediated LTD, and deficits in mRNA transport may contribute to the LTD and/or spine phenotypes in KO neurons (Penagarikano et al., 2007). Indeed, we found that a relatively brief suppression of FMRP and target mRNA transport into dendrites caused an alteration of dendritic filopodia-spine protrusions during a period of active synaptogenesis.

Impaired Motor-Dependent Delivery of Dendritic mRNAs in the Absence of FMRP

In the absence of FMRP we discovered marked alterations in activity-induced localization of a subset of mRNAs in neurons. To our knowledge, this study represents the first characterization of an mRNA localization defect in neurons from a mouse knockout for a specific mRBP. A similar effect was reported for *β-actin* mRNA in dendrites after knockdown of either ZBP1 or Staufen2 in neurons (Eom et al., 2003; Goetze et al., 2006). Our use of MS2-GFP tethered to the *CaMKIIα* 3′UTR, coupled with an automated particle tracking program, represents a significant advance in the ability to monitor mRNA dynamics in living neurons. In support of the FISH studies, the biophysical data solidify the finding of altered mRNA trafficking in dendrites of KO neurons in response to activation of mGluR. *CaMKIIα* is a particularly good example of a dendritic mRNA that associates with FMRP (Muddashetty et al., 2007; Zalfa et al., 2003), and its 3′UTR is sufficient for regulated dendritic trafficking (Rook et al., 2000). Previous reports implicate CaMKIIα protein function in the attenuation of DHPG-induced LTD in the CA1 region of hippocampus (Schnabel et al., 1999), and perhaps failed delivery of *CaMKIIα* mRNA into dendrites contributes to exaggerated LTD observed in the KO mouse. Interestingly, a mouse KO of the *CaMKIIα* mRBP translin exhibits defects in learning and memory and increased epilepsy similar to the *KO* mouse (Stein et al., 2006). Translin may function in the constitutive pathway for *CaMKIIα* mRNA localization that contributes to basal levels of CaMKIIα in dendrites since its disruption affects unstimulated neurons (Severt et al., 1999), whereas we observe no reduction in constitutively localized *CaMKIIα* mRNA in *Fmr1* KO neurons, as previously reported (Steward et al., 1998). In addition, diminished synaptic CaMKIIα protein contributes to learning deficits and epilepsy in a mouse model of Angelman syndrome (Weeber et al., 2003), providing yet a further example that CaMKIIα may be a common target among diverse autism spectrum disorders.

Activity-dependent targeting of mRNAs to specific synaptic sites is important for long-lasting forms of plasticity (Steward and Worley, 2001). Mislocalization of FMRP target mRNAs has direct implications for altered synapse structure and signaling, such as *MAP1b* (Davidkova and Carroll, 2007) which can modify AMPA-R endocytosis and *RGS5*, belonging to a family of G protein regulators implicated in hyperactive mGluR signaling (Saugstad et al., 1998). *SAPAP4* mRNA has not previously been shown to localize to dendrites, and may function in establishment of early postsynaptic structures that target AMPA receptors (Bresler et al., 2001). Diminished stimulus-induced localization of *GABAR-δ* mRNA is consistent with the decreased protein measured in KO mouse brain (D'Hulst et al., 2006) and has relevant implications for the pathology of FXS (Spigelman et al., 2002). Another proposed mRNA target of FMRP is *Arc* (Zalfa et al., 2003), but its localization in KO neurons was apparently not different from WT, consistent with previous reports (Steward et al., 1998). Other mRBPs may mediate mRNA transport via alternate signaling pathways in the absence of FMRP (Steward et al., 1998), such

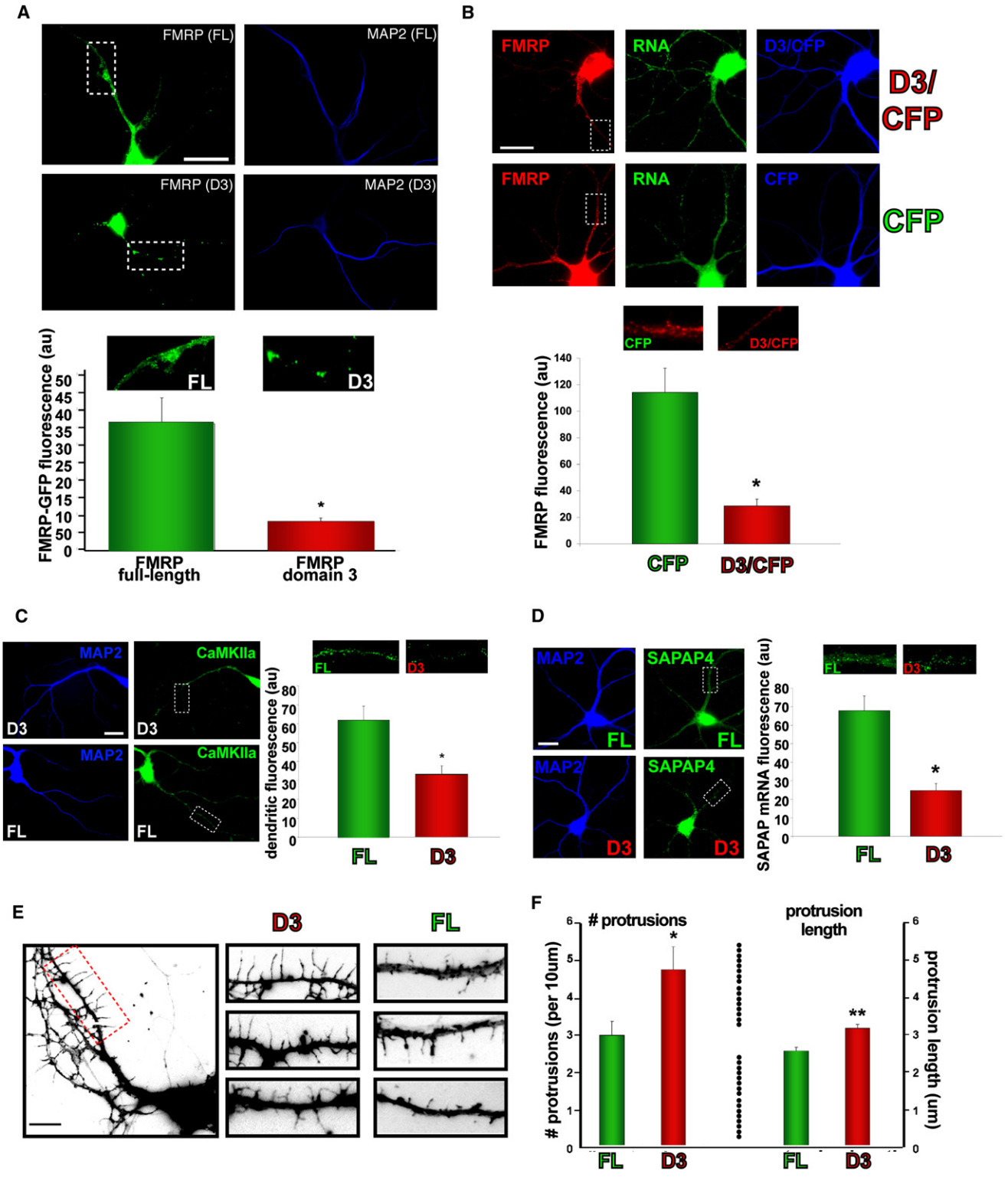

Figure 5. FMRP and Target mRNA Transport Regulates the Length and Number of Dendritic Filopodia-Spine Protrusions

(A and B) Overexpression of the C-terminal domain (D3) of FMRP in hippocampal neurons.

(A) Cultured neurons (11 DIV) were transfected with constructs bearing either FL-FMRP (upper panels) or the C-terminal domain (D3, lower panels) as FLAG-tagged proteins along with FMRP-GFP as a reporter for dendritic transport. GFP fluorescence (left panels) and MAP2 staining (right panels) are shown for representative images. The histogram (below) indicates the average fluorescence intensities of FMRP-GFP in dendrites of treated cells (n = 20–23; *p < 0.002; values shown are mean ± SEM), with images showing blow-up regions of corresponding dendritic FMRP-GPF outlined in the whole cell images (above). Scale bar = 15 μM.

as translin (Severt et al., 1999) or CPEB (Huang et al., 2002), which are both implicated in *CaMKIIα* mRNA localization. Thus while excess mRNA translation at basal states contributes to altered synaptic function in FXS (Muddashetty et al., 2007), an additional deficit is the impaired delivery of specific mRNAs in response to mGluR.

Although microtubule motors have been implicated in mRNP trafficking to dendrites (Kanai et al., 2004), the mechanism of regulation remains unknown. The data here support a model placing the interactions between an mRBP, such as FMRP, and KIF5 downstream of a glutamate receptor. The C-terminal domain of FMRP (D3; Figures 1 and 6, and Figure S2) associates with KIF5 through KLC, which may be a unique interaction given the divergence of the C terminus compared to its close homologs FXR1p and FXR2p. This region also interacts with Ran-binding protein that directly binds to KLC (Menon et al., 2004). Although KLC may be dispensable for transport of the *Drosophila* homolog of FMRP (dFMR) in cultured S2 cells, KLC function is essential for KIF5-mediated transport in mammalian neurons (Rahman et al., 1999), and our data extend KLC function to neuronal mRNA granule transport.

Transport of Dendritic mRNAs Important for Filopodial-Spine Dynamics

In support of a model whereby FMRP functions as a structural adaptor, we found reduced association of FMRP-specific mRNAs with KIF5 in *Fmr1* KO brain (Figure 4). However, none of the mRNAs were completely dissociated, demonstrating a role for other mRBPs in this function. We speculate that defects in the regulated dynamics of mRNA transport may contribute, in part, to the spine phenotype in FXS. For example, since regulators of actin dynamics mediate spine shrinkage during LTD, *RIP (p116)* function in F-actin regulation through Rho (Mulder et al., 2004) may induce newly formed long filopodia or spines, while diminished targeting of *RIP* mRNA could lead to destabilization of actin and block spine maturation. Localized *cofilin phosphatase (PP2Ac)* mRNA (Castets et al., 2005) may also be critical to regulate local actin dynamics and spine morphology in response to synaptic activity.

In an attempt to link mRNA localization defects to alterations in spine morphology in FXS, we disrupted transport in WT neurons during a period of development enriched in filopodial protrusions that may be precursors to spines (Bonhoeffer and Yuste, 2002). Acute disruption of FMRP (36 hr) caused a significant increase in the length and density of dendritic filopodia-spine protrusions (Figure 5) that was strikingly similar to FXS. Since filopodia-spines can elongate rapidly in response to the same glutamatergic stimulus that induces FMRP and target mRNA localization (Vanderklish and Edelman, 2002), our results suggest that the exaggerated morphologic response in KO neurons is directly related to mRNA delivery. We speculate that an acute loss of stimulus-induced *CaMKIIα* and *SAPAP4* mRNA localization to synapses (Figure 5), for example, could account for the persistence of filopodial protrusions that fail to mature into spine synapses (Jourdain et al., 2003).

FMRP Links mGluR-Induced Dendritic mRNA Transport to Local Translation

Taken together, our results on mGluR-regulated mRNA localization defects in KO neurons, in combination with documented defects in translation, suggest a model that couples stimulus-induced mRNA transport to localized translation and synaptogenesis (Figure 6). In this model, neurons under basal conditions constitutively target mRNAs that transport via alternative mRBPs and arrive at the synapse where they are normally repressed by FMRP, but in its absence are translated precociously (as in FXS). Upon enhanced mGluR stimulation in WT neurons synaptic derepression of FMRP allows mRNAs to be translated while somatic FMRP becomes highly engaged in transport of additional mRNAs to dendrites. Over longer periods of time, recurrent glutamatergic stimulation driving synapse formation during development may lead to preferential capture of mRNAs at certain synapses. In neurons without FMRP, the inability to differentially augment targeted mRNA transport to specific synapses may result in a lack of activity-dependent local protein synthesis and lead to dysregulated synapse-specific and neuron-wide plasticity in response to stimulation. This lack of differential selection for synaptogenic potential may be similar to other defects in homeostatic synaptic control that are hallmarks of related neurological syndromes, such as Rett (Dani et al., 2005). The present study has identified several key FMRP targets that are dysregulated in dendrites and may provide insight into new therapeutics for

(B) Staining of endogenous FMRP after overexpression of D3-FMRP (with CFP as marker). Neurons were stained for endogenous FMRP (red images; using an antibody that does not recognize domain 3 (D3) of FMRP), total RNA (green images; SYTO-Select), and cotransfected CFP is shown (blue). FMRP IF was quantified in dendrites (histogram, below) for both D3 neurons (upper panels, D3/CFP) and control transfected neurons (lower panels, CFP). (n = 15–22; *p < 0.001; values shown are mean ± SEM). Blow-up images above the histogram bars show the corresponding outlined regions of the whole cell images (above). Scale bar = 15 μm.

(C) Dendritic CaMKIIα mRNA localization in response to DHPG (11DIV). Representative images are shown (left) for MAP2 staining (blue) and CaMKIIα mRNA FISH (green) for both D3 (upper panels) and FL FMRP (lower panels) overexpression. Histogram (right) shows quantification of dendritic fluorescence of CaMKIIα (n = 13; *p < 0.01; values shown are mean ± SEM), with blow-up images above bars showing dendritic regions outlined in the whole cell images (above). Scale bar = 10 μm.

(D) Dendritic SAPAP4 mRNA localization in response to DHPG (11DIV). Representative images are shown (left) for MAP2 staining (blue) and SAPAP4 mRNA FISH (green) for both D3 (lower panels) and FL FMRP (upper panels) overexpression. Histogram (right) shows quantification of dendritic fluorescence of SAPAP4 (n = 14–15; *p < 0.001; values shown are mean ± SEM), with blow-up images above bars showing outlined dendritic regions outlined in whole cell images (above). Scale bar = 10 μm.

(E and F) Dendritic filopodia-spine protrusion analysis in response to DHPG.

(E) Actin-CFP staining (10 DIV) cotransfected with either D3 or FL FMRP highlights dendritic filopodia-spine protrusion morphology. A representative neuron with D3 overexpression is shown at left, with blow-up panels from representative dendrites at right for both treatments. Scale bar = 5 μm.

(F) Histogram showing quantification of dendritic filopodia-spine protrusion number and lengths in D3 or FL FMRP neurons (n = 749–852 protrusions measured; *p < 0.005 for # protrusions; **p < 0.0001 for protrusion length; values shown are mean ± SEM).

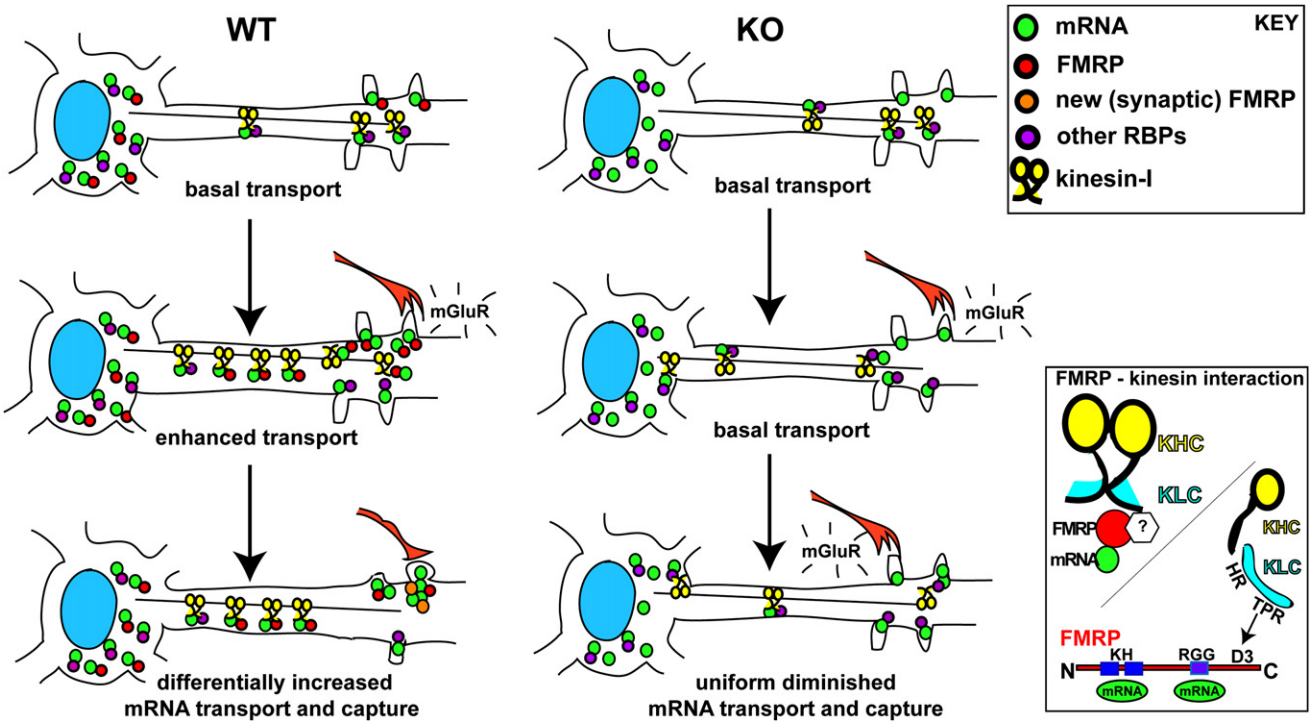

Figure 6. Model for FMRP Function in Linking Stimulus-Induced Dendritic mRNA Transport to Local Translation at Filopodia-Spines to Achieve Proper Synaptic Maturation

mGluR activation causes a differential accumulation and subsequent translation of mRNAs important for synapse formation and maturation during development in WT neurons, but in neurons lacking FMRP this selective transport-dependent increase in mRNAs is dysregulated. As a result, there is a gross lack of maturation of activated filopodia-spines, leading to increased numbers of immature protrusions. These protrusions may persist since translation of mRNAs brought by other RBPs is increased in the absence of FMRP. (Inset) Molecular mechanism of KIF5-mediated FMRP-mRNP transport involves an interaction of the TPR domain of KLC with the C terminus (D3) of FMRP, although this may not necessarily be a direct interaction. Other unknown (?) proteins may be intermediate in this interaction.

the treatment of FXS that target the mRNA localization pathway and its signaling components.

EXPERIMENTAL PROCEDURES

Animals, Cell Culture, and Drug Treatments

Wild-type and KO FMR1 mice (C57Bl6) were from Jackson Labs. Hippocampal neurons from P0 mice were cultured as described (Antar et al., 2004). Cortical neurons from P0 mice were plated at a density of $\sim 2 \times 10^6$ (10 cm dish). DHPG (Tocris) was added to the medium for the indicated times before fixation. For cytoskeletal disruption, either nocodazole (Sigma; 2 μg/ml) or latrunculin (Sigma; 150 μM) were added to media for 30 min before fixation. For kinesin removal from microtubules, AS-2 (gift, L. Goldstein, University of California, San Diego) was diluted (50 μM final) into prewarmed (37°C) microtubule-stabilizing buffer (MSB; 80 mM PIPES [pH 6.8], 10% glycerol, 2 mM MgCl2, 1 mM EGTA, 1 mM GTP, 0.1% saponin) and immediately used to extract cells for 15 s before fixation in −20°C MeOH.

IF and Antibodies

IF was performed as described (Antar et al., 2004). Kinesin heavy chain (KHC; mouse) and dynein (mouse; clone 74.1) antibodies were from Chemicon. FMRP monoclonal (IC3; Chemicon) and polyclonal (H-120; Santa Cruz Biotech) antibodies were used. Antibodies to MAP2 (mouse), FLAG (rabbit, mouse), and HA (rabbit, mouse) were from Sigma. Antibodies against FXR1p (rabbit) were obtained (gift, E. Khandjian (Laval University). Dendritic RNA was stained with SytoSelect and F-actin was detected with Alexa-488-conjugated phalloidin (Invitrogen). Secondary antibodies against mouse (Cy3) and rabbit (Cy5) were used (Jackson ImmunoResearch). Images captured in three-dimensions were taken using 0.1 μm Z-steps, and deconvolved using AutoQuant (Media Cybernetics). Restored images were analyzed in 3D using Imaris (Bitplane, Inc).

Fluorescence In Situ Hybridization (FISH)

Probes were designed using DNAsis and Oligo 4 against the 3′UTR region of mouse MAP1b and b-actin mRNA as described (Bassell et al., 1998). Coding region probes were designed to the *Fmr1* mRNA as described (Antar et al., 2004). Probes were checked for specificity using BLAST on NCBI. Amino-modified oligos were made on a DNA synthesizer and labeled directly with Cy3 or with digoxigenin succinimide ester (Bassell et al., 1998). Some probes (MAP2, RGS5, SAPAP4, GABA-A-R-δ, Arc, CaMKIIα) were designed to the 3′UTR and directly labeled with Cy3 as described (Shav-Tal et al., 2004). All in situs were carried as out as previously described (Antar et al., 2004). For indirect labeling, hybridized probes were detected by IF using a Cy3-conjugated mouse anti-dig antibody and a Cy3-conjugated anti-mouse IgG antibody (Jackson). For negative controls, sense or scrambled probes were used. For analysis of KLC-TPR on *Fmr1* mRNA, 6 DIV (days in vitro) neurons were transfected with the KLC-TPR-HA construct (or FL-KLC-HA as control) for 16 hr before fixation and FISH. For MS2 FISH experiments neurons were cotransfected with MS2-GFP and CaMKIIα 3′ UTR-MS2 at 7DIV. After 24 hr, the neurons were subjected to FISH with MS2-Cy3 probes and immunostained for endogenous FMRP.

Microtubule Cosedimentation Experiments

Embryonic brain extracts were prepared in MSB with GTP (1 mM) and taxol was added (10 μM) before incubation at RT for 10 min. Extracts were centrifuged and supernatants (SUPS) were used for cosedimentation assays. Taxol

microtubules were made as suggested (Cytoskeleton) and added (0.2 mg/ml) to extracts, supplemented with either ATP (1 mM), AMP-PNP (0.5 mM), or hexokinase (1 μM) plus glucose (1 mM, ATP-depleted) and incubated at 37°C for 15 min before centrifugation through a sucrose cushion (20%) for 20 min at 25,000 × g.

Live Cell Imaging of FMRP-GFP and FRAP

For live cell particle tracking, CMV-pEGFP-FMRP was transfected into cultured rat hippocampal neurons and imaged 12–16 hr later. Images were captured with a Nikon Eclipse inverted microscope with 1 s shutter intervals using IP Lab Software (Scanalytics) and analyzed as described (Tiruchinapalli et al., 2003). For FRAP analysis, neurons were transfected with EGFP-FMRP driven by the FMR1 promoter (gift, J. Darnell, Rockefeller University) and either FL-KLC or TPR-KLC as HA-fusion proteins (gift, B. Schnapp, Oregon Health & Science University.) and imaged 12–16 hr later. Dendritic FMRP was subjected to FRAP analysis as described previously (Antar et al., 2004) and calculated recovery rates determined.

Neuronal Transfections and In Vivo Domain Analysis

Neurons were transfected between 3–11 DIV using Lipofectamine 2000 as suggested (Invitrogen). For analysis of kinesin interacting domains, FLAG-FMRP constructs were cotransfected with full-length EGFP-FMRP (FMR1 promoter) at a ratio of 5:1 (FLAG:GFP constructs) to determine the effect of domain overexpression on transport into dendrites. For analysis of dendritic filopodia-spine protrusions, neurons were transfected both with CFP-β-actin and either FMRP-D3-FLAG or FMRP-FL-FLAG at a ratio of 1:5. Neurons were subjected to IF to identify dendrites using anti-MAP2 antibody staining.

FMRP Domain Constructs

Domains of FMRP as FLAG-tagged fusion proteins were subcloned by PCR using primers that contained EcoRI (5′) and SalI (3′) sites in the pcDNA3.1(+) vector (Invitrogen) driven by the CMV promoter containing a FLAG-fusion at the N terminus. FMRP domains contained amino acids 1–208 (domain 1-FMRP), 209–386 (domain 2-FMRP), and 387–615 (domain 3-FMRP).

Dendritic Filopodia-Spine Protrusion Analysis

Quantification of dendritic filopodia-spines was performed on CFP-β-actin transfected images that were chosen randomly from a series of collected neurons (at least 13 per treatment) from coverslips obtained from at least three separate hippocampal cultures. After transfection of CFP-β-actin and either D3-FMRP or FL-FMRP and fixation (36 hr), neurons were costained for MAP2 and synapsin to identify dendrites and synapses. Quantification of protrusion length was done using IPlab software, and measurements for total protrusion density were performed by dividing the total number of protrusions by the length of total dendrite lengths measured, expressed ultimately per 10 μm of dendrite. All protrusions, either in contact with presynaptic terminals or not, were counted as filopodia-spines as previously described (Prange and Murphy, 2001).

Immunoprecipitations (IP) and Western Blotting

For FMRP domain analysis, KLC-HA and either full-length FMRP-FLAG or domains of FMRP-FLAG constructs were cotransfected into human embryonic kidney (HEK293) cell lines for 48–72 hr, lysed in COIP buffer (50 mM Tris-Cl [pH 7.3], 100 mM NaCl, 2 mM MgCl2, 1 mM EDTA, 5% glycerol) and 1 mM ATP for 20 min on ice, and then supernatants (SUPS) isolated by centrifugation (16,000 × g) for 10 min at 4°C. SUPS were IP by mouse anti-FLAG beads (Sigma) for 2–12 hr at 4°C. To resolve FLAG-FMRP-domains from comigrating IgG light chains on SDS-PAGE, blots were probed with mouse anti-HA and rabbit anti-FLAG (Sigma).

Cortical neurons were either not stimulated or stimulated with DHPG for 15 min before solubilization in COIP buffer and subjected to centrifugation. SUPS were IP with anti-KHC antibody coupled to protein G-sepharose at 4°C, isolated, and processed similar to FLAG proteins (above) for SDS-PAGE analysis. IPs of kinesin and FMRP from mouse brain used an established IP protocol for FMRP (Brown et al., 2001) with some modification. Two ml of lysate (w/2 mM ATP) was IP with 10 μg 7G1-1 (mouse anti-FMRP; gift, S. Warren, Emory University) or 10 μg anti-KHC conjugated to 60 μl of protein A sepharose (Pharmacia). Total brain IP of KHC, KIF3, and dynein (anti-74.1) were performed similarly with control (nonspecific IgG) antibodies. Lysates were IP for 3–12 hr and washed with excess lysis buffer. RNase-free DNase I (50 U) was added during the last wash. Western blots used α-tubulin (Sigma), FLAG (Sigma; mouse, rabbit), KIF5 (Covance), and dynein IC (anti-74.1; Sigma) at 1:3000, 1:1000, 1:500, and 1:1000, respectively.

RT-PCR and Quantitative Real-Time PCR, Q-PCR

For semi-Q RT-PCR analysis of motor-associated RNAs, the IP pellets (see kinesin IPs above) were resuspended in DEPC-H20 supplemented with RNase inhibitor, a fraction was set aside for protein analysis (10%), and the remaining pellet was extracted using Trizol (GIBCO BRL). RNA pellets were resuspended in RNase-free H_2O, supplemented with RNase inhibitor, and then used for RT (SuperScript First Strand Synthesis, Invitrogen) coupled with PCR using specific primers for the genes indicated. For the RT step, 1.1 μg RNA was used for each sample, and oligo-dT was used as primer. All amounts of RNA or cDNA were determined by UV-spec analysis (NanoDrop). For RT-PCR, 10% of the RT product (cDNA; 2 μl) was used with gene-specific primers (see the Supplemental Experimental Procedures) and performed as described previously (Zhang et al., 2001). For Q-PCR, 400 ng of each cDNA was used for each reaction. Reactions used Taqman PCR Master Mix (Appl. Biosys.), each cDNA tested in quadruplicate in two experiments. Taqman gene probes (Appl. Biosys.) were used as suggested. Real-time analysis was performed at the AECOM DNA Facility (Appl. Biosys. 7500), and each mRNA (cycle-time) was analyzed at a threshold value (0.2) where all samples were in the linear range of amplification. Quantification of relative amounts of mRNA was performed using the ΔΔCt method, with background subtracted using values from anti-FMRP pellets in KO brain.

Quantification and Image Analysis

Dendritic quantification of fluorescence was performed on images taken with the same exposure times and within the same experiment using IP lab (Scanalytics) software. Total fluorescence was measured by tracing a defined region of interest (ROI) and the fluorescence normalized for area. Dendrites were chosen by DIC and traces were transferred to the corresponding fluorescence images to remove bias; dendrites segments (1–3 per neuron) were taken from regions at least 10 μm away from the cell body and up to 80 μm away from the cell body. Background (normalized for area) from regions on the coverslips outside the cell were subtracted from each dendritic measurement to attain an average dendritic intensity. 3D reconstructions and colocalizations were performed using Imaris software (Tiruchinapalli et al., 2003). Pearson's correlation coefficient was calculated using Costes' algorithm (to minimize noise contribution; ImageJ, NIH) for each dendritic segment obtained from the 3D-reconstructed images for each antigen (FMRP, KIF5, KIF2). All histograms show mean values with error bars reflecting the calculated standard error of the mean. The indicated total number of cells (n) analyzed for each experiment are shown in the figure legends, and all statistical measurements were performed using Student's t test (unpaired). Data were derived from at least three separate experiments unless stated otherwise.

MS2-GFP mRNA Tracking Experiments

MS2-GFP was transfected into neurons along with the lacZ-plasmid containing eight repeats of MS2-hairpin binding sites fused to the 3′UTR of CaMKIIα mRNA, as previously described (Rook et al., 2000). Briefly, 6 μg of MS2-CaMKIIα-lacZ (gift, K. Kosik, University of California, Santa Barbara) and 2 μg of MS2-GFP were transfected and neurons were imaged 12–16 hr later (see live cell imaging of FMRP-GFP). Transfected cells were identified and dendritic granules imaged for 2 min intervals at 1.5 s per frame (80 frames total). Wild-type and KO neurons were imaged similarly, and movies were submitted to the Localize program (R.H. Singer Lab), which tracked particles above background using identical thresholding parameters for all cells. Mean-squared displacement was calculated and each trajectory graphed accordingly. The computer-based program Localize was used to calculate dynamics based on the algorithm as described (Thompson et al., 2002). Particles were defined as motile only if they met strict criteria of active transport based on previously calculated rates of diffusion of an MS2-GFP mRNA of similar mass (Shav-Tal et al., 2004). For our purposes, we assumed that these rates would be at least in excess of 2-fold of the diffusion rates for at least 6 frames.

SUPPLEMENTAL DATA

Supplemental Data include Supplemental Experimental Procedures, six figures, and three movies, and are available with this article online at http://www.developmentalcell.com/cgi/content/full/14/6/926/DC1/.

ACKNOWLEDGMENTS

We thank Dan Larson for help with Localize and single mRNA particle analysis, Shailesh Shenoy for help with microscopy and image analysis, Ines Petersen for FMRP domain analysis in KLC binding, Daniel Cuzzone for technical help, and Chanxia Li for *Fmr1* KO cultures. This work was supported by FRAXA (J.B.D., L.N.A., and G.J.B.), a NFXF Basic Science Grant to J. Dictenberg, NIH AR-41480 to R.H. Singer, and NIH NS051127 and Dana Foundation to G.J. Bassell. J.B. Dictenberg is a recipient of the Albert Einstein Scholar Award.

Received: November 29, 2007
Revised: March 19, 2008
Accepted: April 16, 2008
Published: June 9, 2008

REFERENCES

Antar, L.N., Afroz, R., Dictenberg, J.B., Carroll, R.C., and Bassell, G.J. (2004). Metabotropic glutamate receptor activation regulates fragile x mental retardation protein and FMR1 mRNA localization differentially in dendrites and at synapses. J. Neurosci. *24*, 2648–2655.

Antar, L.N., Dictenberg, J.B., Plociniak, M., Afroz, R., and Bassell, G.J. (2005). Localization of FMRP-associated mRNA granules and requirement of microtubules for activity-dependent trafficking in hippocampal neurons. Genes Brain Behav. *4*, 350–359.

Aschrafi, A., Cunningham, B.A., Edelman, G.M., and Vanderklish, P.W. (2005). The fragile X mental retardation protein and group I metabotropic glutamate receptors regulate levels of mRNA granules in brain. Proc. Natl. Acad. Sci. USA *102*, 2180–2185.

Bagni, C., and Greenough, W.T. (2005). From mRNP trafficking to spine dysmorphogenesis: the roots of fragile X syndrome. Nat. Rev. Neurosci. *6*, 376–387.

Bassell, G.J., Zhang, H., Byrd, A.L., Femino, A.M., Singer, R.H., Taneja, K.L., Lifshitz, L.M., Herman, I.M., and Kosik, K.S. (1998). Sorting of β-actin mRNA and protein to neurites and growth cones in culture. J. Neurosci. *18*, 251–265.

Bonhoeffer, T., and Yuste, R. (2002). Spine motility. Phenomenology, mechanisms, and function. Neuron *35*, 1019–1027.

Bramham, C.R., and Wells, D.G. (2007). Dendritic mRNA: transport, translation and function. Nat. Rev. Neurosci. *8*, 776–789.

Bresler, T., Ramati, Y., Zamorano, P.L., Zhai, R., Garner, C.C., and Ziv, N.E. (2001). The dynamics of SAP90/PSD-95 recruitment to new synaptic junctions. Mol. Cell. Neurosci. *18*, 149–167.

Brown, V., Jin, P., Ceman, S., Darnell, J.C., O'Donnell, W.T., Tenenbaum, S.A., Jin, X., Feng, Y., Wilkinson, K.D., Keene, J.D., et al. (2001). Microarray identification of FMRP-associated brain mRNAs and altered mRNA translational profiles in fragile X syndrome. Cell *107*, 477–487.

Carrington, W.A., Lynch, R.M., Moore, E.D., Isenberg, G., Fogarty, K.E., and Fay, F.S. (1995). Superresolution three-dimensional images of fluorescence in cells with minimal light exposure. Science *268*, 1483–1487.

Castets, M., Schaeffer, C., Bechara, E., Schenck, A., Khandjian, E.W., Luche, S., Moine, H., Rabilloud, T., Mandel, J.L., and Bardoni, B. (2005). FMRP interferes with the Rac1 pathway and controls actin cytoskeleton dynamics in murine fibroblasts. Hum. Mol. Genet. *14*, 835–844.

Ceman, S., Brown, V., and Warren, S.T. (1999). Isolation of an FMRP-associated messenger ribonucleoprotein particle and identification of nucleolin and the fragile X-related proteins as components of the complex. Mol. Cell. Biol. *19*, 7925–7932.

D'Hulst, C., De Geest, N., Reeve, S.P., Van Dam, D., De Deyn, P.P., Hassan, B.A., and Kooy, R.F. (2006). Decreased expression of the GABAA receptor in fragile X syndrome. Brain Res. *1121*, 238–245.

Dani, V.S., Chang, Q., Maffei, A., Turrigiano, G.G., Jaenisch, R., and Nelson, S.B. (2005). Reduced cortical activity due to a shift in the balance between excitation and inhibition in a mouse model of Rett syndrome. Proc. Natl. Acad. Sci. USA *102*, 12560–12565.

Davidkova, G., and Carroll, R.C. (2007). Characterization of the role of microtubule-associated protein 1B in metabotropic glutamate receptor-mediated endocytosis of AMPA receptors in hippocampus. J. Neurosci. *27*, 13273–13278.

Dictenberg, J.B., and Singer, R.H. (2008). Dendritic RNA transport: dynamic spatio-temporal control of neuronal gene expression. In Encyclopedia of Neuroscience, L.R. Squire, ed. (Oxford: Academic Press).

Eom, T., Antar, L.N., Singer, R.H., and Bassell, G.J. (2003). Localization of a β-actin messenger ribonucleoprotein complex with zipcode-binding protein modulates the density of dendritic filopodia and filopodial synapses. J. Neurosci. *23*, 10433–10444.

Goetze, B., Tuebing, F., Xie, Y., Dorostkar, M.M., Thomas, S., Pehl, U., Boehm, S., Macchi, P., and Kiebler, M.A. (2006). The brain-specific double-stranded RNA-binding protein Staufen2 is required for dendritic spine morphogenesis. J. Cell Biol. *172*, 221–231.

Gold, S.J., Ni, Y.G., Dohlman, H.G., and Nestler, E.J. (1997). Regulators of G-protein signaling (RGS) proteins: region-specific expression of nine subtypes in rat brain. J. Neurosci. *17*, 8024–8037.

Huang, Y.S., Jung, M.Y., Sarkissian, M., and Richter, J.D. (2002). N-methyl-D-aspartate receptor signaling results in Aurora kinase-catalyzed CPEB phosphorylation and α CaMKII mRNA polyadenylation at synapses. EMBO J. *21*, 2139–2148.

Jourdain, P., Fukunaga, K., and Muller, D. (2003). Calcium/calmodulin-dependent protein kinase II contributes to activity-dependent filopodia growth and spine formation. J. Neurosci. *23*, 10645–10649.

Kanai, Y., Dohmae, N., and Hirokawa, N. (2004). Kinesin transports RNA: isolation and characterization of an RNA-transporting granule. Neuron *43*, 513–525.

Kiebler, M.A., and Bassell, G.J. (2006). Neuronal RNA granules: movers and makers. Neuron *51*, 685–690.

Lu, R., Wang, H., Liang, Z., Ku, L., O'Donnell, W.T., Li, W., Warren, S.T., and Feng, Y. (2004). The fragile X protein controls microtubule-associated protein 1B translation and microtubule stability in brain neuron development. Proc. Natl. Acad. Sci. USA *101*, 15201–15206.

Menon, R.P., Gibson, T.J., and Pastore, A. (2004). The C terminus of fragile X mental retardation protein interacts with the multi-domain Ran-binding protein in the microtubule-organising centre. J. Mol. Biol. *343*, 43–53.

Miller, S., Yasuda, M., Coats, J.K., Jones, Y., Martone, M.E., and Mayford, M. (2002). Disruption of dendritic translation of CaMKIIα impairs stabilization of synaptic plasticity and memory consolidation. Neuron *36*, 507–519.

Miyashiro, K.Y., Beckel-Mitchener, A., Purk, T.P., Becker, K.G., Barret, T., Liu, L., Carbonetto, S., Weiler, I.J., Greenough, W.T., and Eberwine, J. (2003). RNA cargoes associating with FMRP reveal deficits in cellular functioning in *Fmr1* null mice. Neuron *37*, 417–431.

Muddashetty, R.S., Kelic, S., Gross, C., Xu, M., and Bassell, G.J. (2007). Dysregulated metabotropic glutamate receptor-dependent translation of AMPA receptor and postsynaptic density-95 mRNAs at synapses in a mouse model of fragile X syndrome. J. Neurosci. *27*, 5338–5348.

Mulder, J., Ariaens, A., van den Boomen, D., and Moolenaar, W.H. (2004). p116Rip targets myosin phosphatase to the actin cytoskeleton and is essential for RhoA/ROCK-regulated neuritogenesis. Mol. Biol. Cell *15*, 5516–5527.

Penagarikano, O., Mulle, J.G., and Warren, S.T. (2007). The pathophysiology of fragile x syndrome. Annu. Rev. Genomics Hum. Genet. *8*, 109–129.

Prange, O., and Murphy, T.H. (2001). Modular transport of postsynaptic density-95 clusters and association with stable spine precursors during early development of cortical neurons. J. Neurosci. *21*, 9325–9333.

Rahman, A., Kamal, A., Roberts, E.A., and Goldstein, L.S. (1999). Defective kinesin heavy chain behavior in mouse kinesin light chain mutants. J. Cell Biol. *146*, 1277–1288.

Rook, M.S., Lu, M., and Kosik, K.S. (2000). CaMKIIα 3′ untranslated region-directed mRNA translocation in living neurons: visualization by GFP linkage. J. Neurosci. *20*, 6385–6393.

Sakowicz, R., Berdelis, M.S., Ray, K., Blackburn, C.L., Hopmann, C., Faulkner, D.J., and Goldstein, L.S. (1998). A marine natural product inhibitor of kinesin motors. Science *280*, 292–295.

Saugstad, J.A., Marino, M.J., Folk, J.A., Hepler, J.R., and Conn, P.J. (1998). RGS4 inhibits signaling by group I metabotropic glutamate receptors. J. Neurosci. *18*, 905–913.

Schnabel, R., Palmer, M.J., Kilpatrick, I.C., and Collingridge, G.L. (1999). A CaMKII inhibitor, KN-62, facilitates DHPG-induced LTD in the CA1 region of the hippocampus. Neuropharmacology *38*, 605–608.

Severt, W.L., Biber, T.U., Wu, X., Hecht, N.B., DeLorenzo, R.J., and Jakoi, E.R. (1999). The suppression of testis-brain RNA binding protein and kinesin heavy chain disrupts mRNA sorting in dendrites. J. Cell Sci. *112*, 3691–3702.

Shav-Tal, Y., Darzacq, X., Shenoy, S.M., Fusco, D., Janicki, S.M., Spector, D.L., and Singer, R.H. (2004). Dynamics of single mRNPs in nuclei of living cells. Science *304*, 1797–1800.

Spigelman, I., Li, Z., Banerjee, P.K., Mihalek, R.M., Homanics, G.E., and Olsen, R.W. (2002). Behavior and physiology of mice lacking the GABAA-receptor delta subunit. Epilepsia *43* (*Suppl 5*), 3–8.

Stein, J.M., Bergman, W., Fang, Y., Davison, L., Brensinger, C., Robinson, M.B., Hecht, N.B., and Abel, T. (2006). Behavioral and neurochemical alterations in mice lacking the RNA-binding protein translin. J. Neurosci. *26*, 2184–2196.

Steward, O., and Worley, P.F. (2001). A cellular mechanism for targeting newly synthesized mRNAs to synaptic sites on dendrites. Proc. Natl. Acad. Sci. USA *98*, 7062–7068.

Steward, O., Bakker, C.E., Willems, P.J., and Oostra, B.A. (1998). No evidence for disruption of normal patterns of mRNA localization in dendrites or dendritic transport of recently synthesized mRNA in FMR1 knockout mice, a model for human fragile-X mental retardation syndrome. Neuroreport *9*, 477–481.

Takeuchi, M., Hata, Y., Hirao, K., Toyoda, A., Irie, M., and Takai, Y. (1997). SAPAPs. A family of PSD-95/SAP90-associated proteins localized at postsynaptic density. J. Biol. Chem. *272*, 11943–11951.

Thompson, R.E., Larson, D.R., and Webb, W.W. (2002). Precise nanometer localization analysis for individual fluorescent probes. Biophys. J. *82*, 2775–2783.

Tiruchinapalli, D.M., Oleynikov, Y., Kelic, S., Shenoy, S.M., Hartley, A., Stanton, P.K., Singer, R.H., and Bassell, G.J. (2003). Activity-dependent trafficking and dynamic localization of zipcode binding protein 1 and β-actin mRNA in dendrites and spines of hippocampal neurons. J. Neurosci. *23*, 3251–3261.

Vanderklish, P.W., and Edelman, G.M. (2002). Dendritic spines elongate after stimulation of group 1 metabotropic glutamate receptors in cultured hippocampal neurons. Proc. Natl. Acad. Sci. USA *99*, 1639–1644.

Vanderklish, P.W., and Edelman, G.M. (2005). Differential translation and fragile X syndrome. Genes Brain Behav. *4*, 360–384.

Verhey, K.J., Meyer, D., Deehan, R., Blenis, J., Schnapp, B.J., Rapoport, T.A., and Margolis, B. (2001). Cargo of kinesin identified as JIP scaffolding proteins and associated signaling molecules. J. Cell Biol. *152*, 959–970.

Weeber, E.J., Jiang, Y.H., Elgersma, Y., Varga, A.W., Carrasquillo, Y., Brown, S.E., Christian, J.M., Mirnikjoo, B., Silva, A., Beaudet, A.L., et al. (2003). Derangements of hippocampal calcium/calmodulin-dependent protein kinase II in a mouse model for Angelman mental retardation syndrome. J. Neurosci. *23*, 2634–2644.

Weiler, I.J., Irwin, S.A., Klintsova, A.Y., Spencer, C.M., Brazelton, A.D., Miyashiro, K., Comery, T.A., Patel, B., Eberwine, J., and Greenough, W.T. (1997). Fragile X mental retardation protein is translated near synapses in response to neurotransmitter activation. Proc. Natl. Acad. Sci. USA *94*, 5395–5400.

Zalfa, F., Giorgi, M., Primerano, B., Moro, A., Di Penta, A., Reis, S., Oostra, B., and Bagni, C. (2003). The fragile X syndrome protein FMRP associates with BC1 RNA and regulates the translation of specific mRNAs at synapses. Cell *112*, 317–327.

Zalfa, F., Eleuteri, B., Dickson, K.S., Mercaldo, V., De Rubeis, S., di Penta, A., Tabolacci, E., Chiurazzi, P., Neri, G., Grant, S.G., et al. (2007). A new function for the fragile X mental retardation protein in regulation of PSD-95 mRNA stability. Nat. Neurosci. *10*, 578–587.

Zhang, H.L., Eom, T., Oleynikov, Y., Shenoy, S.M., Liebelt, D.A., Dictenberg, J.B., Singer, R.H., and Bassell, G.J. (2001). Neurotrophin-induced transport of a β-actin mRNP complex increases β-actin levels and stimulates growth cone motility. Neuron *31*, 261–275.